35th Annual International Conference of the IEEE EMBS
Osaka, Japan, 3 - 7 July, 2013

Viscoelastic Interaction between Intraocular Microrobots and Vitreous Humor: A Finite Element Approach

Zhongkui Wang[1], Juho Pokki[2], Olgaç Ergeneman[2], Bradley J. Nelson[2], and Shinichi Hirai[1]

***Abstract*— Vitreous humor exhibits complex biomechanical properties and determination of these properties is essential for designing ophthalmic biomedical microdevices. In this paper, the viscoelastic properties of porcine vitreous humor were studied based on *ex vivo* creep experiments, in which a microrobot was magnetically actuated inside the vitreous. A three-dimensional (3D) finite element (FE) model was proposed to simulate the viscoelastic interaction between the microrobot and porcine vitreous humor. An optimization-based method was employed to estimate the viscoelastic parameters of the vitreous humor. The proposed model successfully validated the experimental measurements. The estimated parameters were compared with published data in literature. The model was then used to study the shape-dependent interaction of the microrobot with the vitreous humor. The methods presented in this paper can be used for the optimization of ophthalmic microrobots and microsurgical tools.**

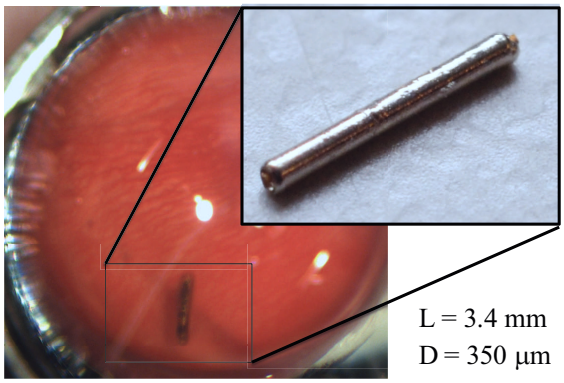

Fig. 1. A cylindrical microrobot moving inside the vitreous humor. The upper right corner shows the microrobot.

I. INTRODUCTION

Vitreous humor is the gel-like fluid that fills the space between the lens and the retina holding the eye. Although it is 99% water, it exhibits one of the most complex biomechanical properties in the body [1]. Understanding the viscoelastic properties of the vitreous humor is essential for designing ophthalmic biomedical devices operating in the posterior segment of the eye. There is a growing interest in devices for pathological diagnosis, minimally-invasive microsurgical tools, and robot-aided tools. Wireless microrobots have also been proposed for ophthalmic applications (Fig. 1) [2], [3]. Design and optimization of these microdevices require thorough knowledge of their viscoelastic interaction with the vitreous humor.

Various methods have been utilized to study the viscoelastic properties of the vitreous humor, such as magnetic tweezers, atomic force microscopy (AFM), particle tracking, and microfluidics [4]. *In-vivo* application of these techniques is not straight-forward. Various attempts to characterize viscoelastic properties of vitreous humor can be found in [1]. A statistically comprehensive investigation was performed by Lee et al using magnetic bead microrheology [5], [6]. Human, bovine, and porcine vitreous humors were cut in parts, and their viscoelastic properties were extracted based on creep measurements. The variation of viscoelastic properties among species and locations (anterior, central, and posterior segments) was discussed. A four-parameter Burgers model was used to describe the viscoelastic behavior of the vitreous humor. Recently, Sharif-Kashani et al. studied the properties of porcine vitreous humor using a stressed-control shear rheometer [1]. The creep deformation was modeled using a five-parameter model (two-element retardation spectrum model) to capture two viscoelastic responses with a short (~ 1 s) and a long time scale (~ 100 s). However, it required excision and segmentation of vitreous humor making it non-applicable *in vivo*.

We have investigated the viscoelastic properties of the vitreous humor by using a magnetic microrobot, which can be controlled with high precision in 3D using a custom electromagnetic manipulation system [2]. A spherical microrobot was utilized for this purpose. The main viscoelastic properties regarding the movement of the microrobot were captured ($\sim$10 s measurements), which arise from the response of collagen fibers (short time scale), and non-relaxed hyalorunan gel and microfibrils (long time scale) [1]. Using this method, Pokki et al. performed creep experiments on both artificial vitreous humor and porcine cadaver vitreous humor [7]. Viscoelastic properties of the vitreous humor were characterized by a curve fitting algorithm. The results were validated by comparing with AFM measurements [7]. This method is promising for *in-vivo* applications since no excision and segmentation are required.

This work builds on the findings of Pokki et al. [7]. The vitreous humor was modeled with a 3D FE method. The viscoelastic parameters of porcine vitreous humor were estimated using the FE model and an optimization-based method. The model was used to evaluate different geometries

*This work was supported by the Research Organization of Science and Technology of Ritsumeikan University and by the NCCR Co-Me of the Swiss National Science Foundation, and an European Research Council Advanced Grant.

[1]Department of Robotics, Ritsumeikan University, 525-8577 Shiga, Japan {wangzk at fc and hirai at se}.ritsumei.ac.jp

[2]Institute of Robotics and Intelligent Systems, ETH Zurich, 8092 Zurich, Switzerland {jpokki and oergeneman and bnelson} at ethz.ch

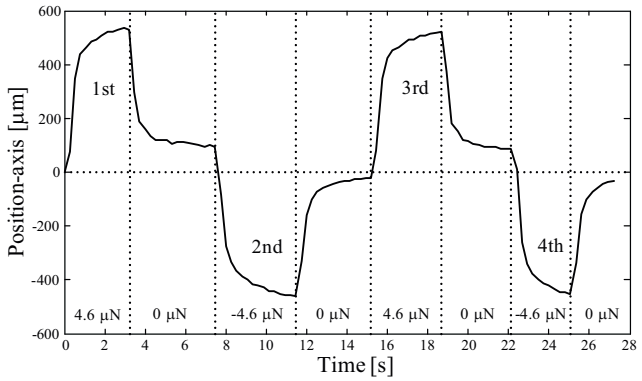

Fig. 2. The experimental measurements of the microrobot trajectory under a cycled stepwise constant magnetic force. Data were adopted from [7].

of ophthalmic microrobots: microsphere, microcylinder, and microellipsoid. Elongated shapes are preferred for the microrobots as they maximize the volume (i.e., magnetic force) while minimizing the cross sectional area, which makes them fit in a needle for minimally-invasive injections. They also exhibit a desirable magnetic shape anisotropy for magnetic manipulation. The ability for translational movement of the different geometries was studied using the developed model.

II. MEASUREMENTS AND METHODS

A. Measurements of Porcine Vitreous Humor

The experimental measurements of porcine vitreous humor published in [7] were used in this paper. A 0.55 mm-diameter NdFeB sphere [Supermagnete, Germany] was driven by magnetic fields to move inside the vitreous humor. A cycled stepwise constant magnetic force ($\pm 4.6\mu$N) was applied on the sphere and the position trajectory of the sphere was tracked [7]. The position measurements of the sphere are shown in Fig. 2. In the following sections, after introducing the FE model and parameter estimation method, viscoelastic properties of the vitreous humor were estimated using the measurements of the first cycle. Measurements of the following cycles were used to validate the estimation results.

B. FE Modeling of Vitreous Humor and the Sphere

In order to describe the viscoelastic properties of vitreous humor, physically based models have been proposed, such as the four-parameter Burgers [5], [6], [7] and five-parameter [1] models. Based on the investigation of the measurements in Fig. 2, we found that a three-parameter Lethersich model (Fig. 3) is suitable for capturing the creep deformation of porcine vitreous humor due to the short time scale for each cycle. In a Lethersich model, the elastic part denoted by Young's modulus E describes the elastic or displacement-dependent properties and the viscous parts denoted by moduli c_1 and c_2 describe the viscous or velocity-dependent properties. A 2D FE formulation with different physical models can be found in [8], which can be extended to a 3D formulation. In this paper, we modeled the vitreous humor using the Lethersich model and modeled the microsphere using a typical elastic model with known parameters of the material. Since the sphere only moves a small distance (about one diameter) and the vitreous humor around the sphere surface moves together with the sphere, we are able to model the vitreous humor with linear FE method and model the interaction between the vitreous and sphere using point-to-point constraints as in [9]. The FE model consists of a set of differential equations which were solved using MATLAB integration algorithm 'ode23' to obtain the displacements and velocities of every nodal points involved in the model. The detailed formulation cannot be presented here due to length.

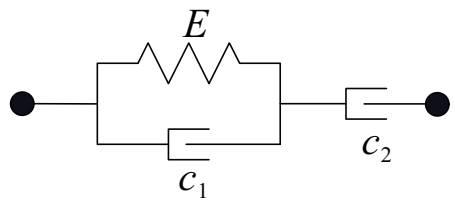

Fig. 3. The three-parameter Lethersich model consists of a Kelvin-Voigt body in series with a dashpot.

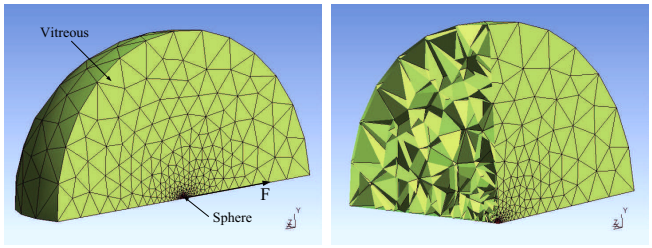

Fig. 4. 3D FE mesh of the vitreous humor and microsphere: (a) overall view and (b) section view. The model was constructed by a set of tetrahedra.

C. FE Mesh Generation

The average size of a porcine eye is approximately 24 mm in diameter [10]. Excluding the sclera, choroid, and retina, we modeled the vitreous humor as a spherical body with a diameter of 20 mm. The microrobot moving inside the vitreous humor was modeled as a small spherical body with a diameter of 0.55 mm. We assume that the force acting on the microsphere is along the x-axis direction (**F** in Fig. 4a) with the microsphere moving along the axis. We modeled a quarter of the vitreous body and microsphere (Fig. 4a) due to symmetry. Boundary constraints were imposed on corresponding nodal points. For example, the nodal points on the xy-plane (horizontal bottom plane) only move in this plane and no z-axis displacements were allowed. Nodal points on spherical surface of the vitreous humor were fixed in space. Figure 4b shows a section view of the mesh. The geometry and FE mesh were generated using 'Gmsh' [11].

D. Parameter Estimation Method

In the FE model, four unknown parameters must be determined, the Young's modulus E, viscous moduli c_1 and c_2, and Poisson's ratio γ which indicates the ratio between lateral strain and normal strain. For incompressible material,

TABLE I

ESTIMATED PARAMETERS OF PORCINE VITREOUS HUMOR AND COMPARISONS WITH PUBLISHED DATA

Parameter	E (Pa)	c_1 (Pa·s)	c_2 (Pa·s)
Value	3.527	1.402	47.370
Ref [1]	1.66±0.96	2.4	70
Ref [6]	0.937±22%	0.599±30%	8.402±36%

the Poisson's ratio usually takes a value close to 0.5. In this work, we set $\gamma = 0.48$ since the vitreous humor has a gel-like property, and we assume it is an incompressible material. Therefore, we have three unknown parameters to be estimated. To this end, we employed the optimization-based method proposed in [8]. The idea is to iterate the FE simulation with updated parameters and minimize the difference of certain physical quantities (trajectory of the microsphere in this work) between experimental measurements and simulation results. This method has been successfully used to estimate the physical parameters of various viscoelastic materials in [12]. The objective function for the optimization problem can be formulated as

$$E(\theta) = \sum_{i=1}^{n} \|x_i^{sim}(\theta) - x_i^{exp}\|^2,$$

where vector $\theta = [E, c_1, c_2]^{\mathrm{T}}$ consists of the parameters to be determined. The positions of the microsphere at the i-th sampling time calculated from simulation and from experimental measurements are x_i^{sim} and x_i^{exp}, respectively. The number of sampling points is n. The threshold used to terminate the optimization is the tolerance on $E(\theta)$ less than 1×10^{-9} or the tolerance on θ less than 1×10^{-6}. The optimization toolbox of MATLAB and 'lsqcurvefit' curve fitting algorithm were used to solve this problem.

III. RESULTS

Using measurements of the first cycle (Fig. 2) as input to the optimization problem, we can minimize the difference of the microsphere trajectories and obtain the viscoelastic parameters of the porcine vitreous humor as given in the first row of Table I. Published data from [1] and [6] are also listed in the second and third rows of Table I for comparison. From Table I we can see that the parameters presented in this paper are significantly larger than the ones in [6] but close to the ones in [1]. The differences are acceptable since the experimental methods and eye samples are different among these works. The proposed model and estimated parameters successfully reproduced the full experimental measurements of four cycles (Fig. 5) including the good prediction of the rest three cycles which validates our method.

The interaction between nonspherical bodies and vitreous humor cannot be easily modeled analytically. The model is used to study the shape-effects of microrobots. Instead of using a microsphere, we modeled the microrobot with prolate microcylinder and microellipsoid (Fig. 6). The ratios

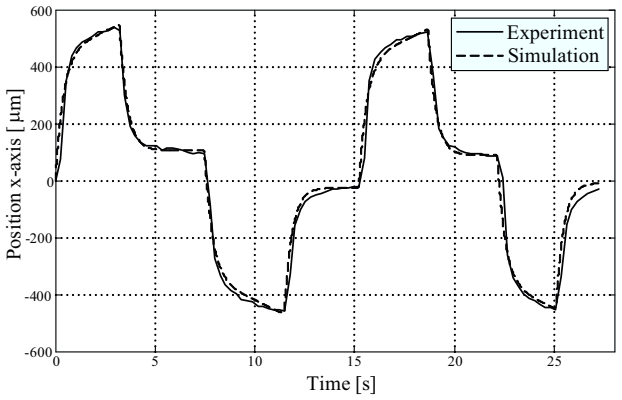

Fig. 5. Simulation results compared with experimental measurements.

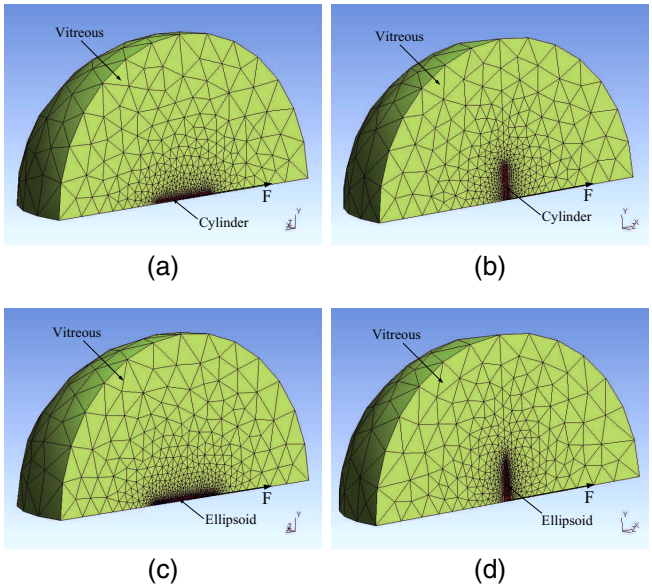

Fig. 6. FE mesh of the vitreous humor with different shaped microrobots and different orientations: (a) horizontal cylinder, (b) vertical cylinder, (c) horizontal ellipsoid, and (d) vertical ellipsoid.

of length-to-diameter for the cylinder and long-to-short semi-principal axes for the ellipsoid were set to 68/7 similar to the intraocular device we are using. We kept the volumes of the microcylinder and microellipsoid the same as the volume of the microsphere. Two configurations were investigated with different orientations of the cylinder and ellipsoid: (1) horizontal orientation, where the longitudinal axes of the microrobots are aligned with the moving direction (Fig. 6a, 6c), (2) vertical orientation, where the longitudinal axes are perpendicular to the moving direction (Fig. 6b, 6d). Moving trajectories of the microrobots were compared in Fig. 7. We can see that the microsphere moves easier than the microellipsoid and microcylinder. The microellipsoid moves slightly easier than the microcylinder. This is because the viscoelastic force (resistance) acting on the microrobot is approximately proportional to the surface area of the robot and the area ratio between three microrobots is sphere/ellipsoid/cylinider $\approx 1/1.684/1.712$. For different orientations of the ellipsoid and cylinder, microrobots with horizontal orientations move

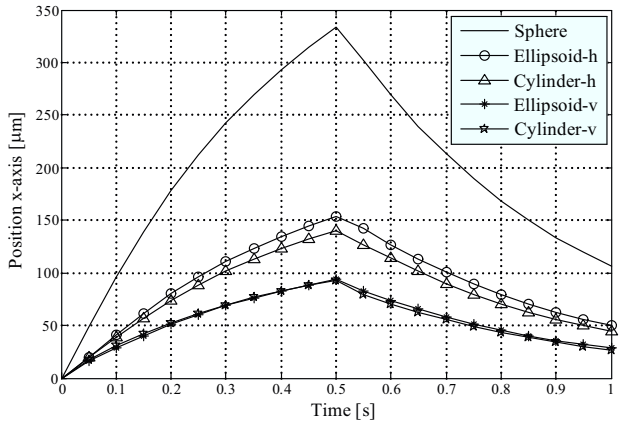

Fig. 7. Trajectory comparisons of different shaped microrobots with different orientations, where '-h' indicates horizontal orientation and '-v' indicates vertical orientation. All microrobots have the same volume.

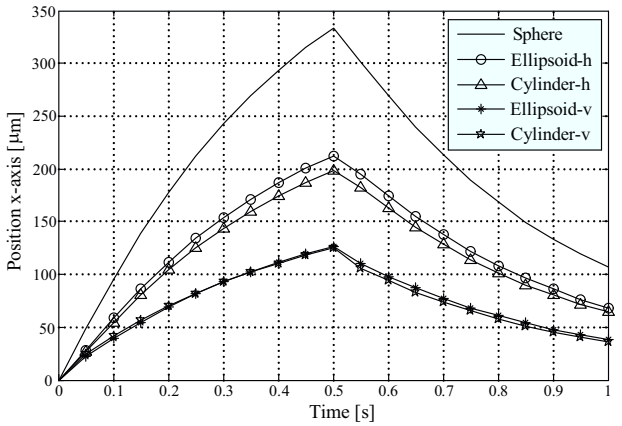

Fig. 8. Trajectory comparisons of different shaped microrobots with different orientations, where '-h' indicates horizontal orientation and '-v' indicates vertical orientation. All microrobots have the same surface area.

easier than robots with vertical orientations. Secondly, we assume that three microrobots have the same surface area and magnetic force but different volumes. Simulation results and comparisons are shown in Fig. 8. The microdevices performed in a similar way as in Fig. 7, which is not as we expected. We can then conclude that other shape factors beyond volume and surface area may also affect microrobots performance.

IV. CONCLUSIONS AND FUTURE WORKS

In this paper, an FE method and a three-parameter Lethersich model were used to model the viscoelastic interaction between porcine vitreous humor and intraocular microrobots. An optimization-based method was employed to estimate the viscoelastic properties of the vitreous humor. The results were compared with the published data from the literature. Simulation results successfully reproduced the experimental measurements and validated the model. The model was then used to study the shape-effects of microrobots. Microcylinder, used for ophthalmic procedures, was compared to microsphere and microellipsoid. We found that the microsphere performed the best among three different geometries and the microellipsoid performed slightly better than the microcylinder. Orientation also affects the performance of the microdevices. In general, the alignment of the longitudinal axis with the moving direction yields better performance. Although the microcylinder did not perform as well as the microsphere or microellipsoid, it is still used for ophthalmic applications because it is easier to fabricate and can maximize the volume while keeping a relatively small diameter to fit in a medical needle. The methods presented in this paper can be used for the optimization of ophthalmic microrobots and microsurgical tools. Other than volume and surface area, other shape factors which may affect the microrobots performance will be studied in the future. The FE model proposed in this paper is a linear model under the assumption of small deformation. Nonlinear models must be studied for large deformation where the microrobots may move with a large displacement to perform a task. In addition, the model is based on solid mechanics. However, the vitreous humor sometimes demonstrates hydrodynamic behaviors and the liquefaction of vitreous humor happens gradually with age. Biological vitreous humor may exhibit properties between those solids and liquids. Therefore, models combining solid and fluid dynamics will be investigated in the future.

REFERENCES

[1] P. Sharif-Kashani, J. Hubschman, D. Sassoon, and H. P. Kavehpour, Rheology of the vitreous gel: effects of macromolecule organization on the viscoelastic properties, J. Biomechanics, 44(3), pp. 419-423, 2011.

[2] M. P. Kummer, J. J. Abbott, B. E. Kratochvil, R. Borer, A. Sengul, and B. J. Nelson, OctoMag: an electromagnetic system for 5-DOF wireless micromanipulation, IEEE Trans. Robotics, 26(6), pp. 1006-1017, 2010.

[3] Y. E. Choonara, V. Pillay, M. P. Danckwerts, T. R. Carmichael, L. C. du Toit, Areview of implantable intravitreal drug delivery technologies for the treatment of posterior segment eye diseases, 99(5), pp. 2219-2239, May 2010.

[4] T. A. Waigh, Microrheology of complex fluids, Reports on Progress in Physics, 68(3), pp. 685-742, 2005.

[5] B. Lee, M. Litt, and G. Buchsbaum, Rheology of the vitreous body. Part I: viscoelasticity of human vitreous, Biorheology, 29, pp. 521-533, 1992.

[6] B. Lee, M. Litt, G. Buchsbaum, Rheology of the vitreous body: Part 2: viscoelasticity of bovine and porcine vitreous, Biorheology, 31(4), pp. 327-338, 1994.

[7] J. Pokki, O. Ergeneman, C. Bergeles, H. Torun, and B. J. Nelson, Localized viscoelasticity measurements with untethered intravitreal microrobots, EMBC2012, San Diego, USA, August 2012.

[8] Z. Wang and S. Hirai, Modeling and parameter identification of rheological object based on FE method and nonlinear optimization, IROS2009, pp. 1968-1973, St. Louis, USA, October 2009.

[9] Z. Wang, L. Wang, V. A. Ho, S. Morikawa, and S. Hirai, A 3d non-homogeneous FE model of human fingertip based on MRI measurements, IEEE Trans. Instrumentation & Measurement, 61(12), pp. 3147-3157, Dec. 2012.

[10] I. Sanchez, R. Martin, F. Ussa, and I. Fernandez-Bueno, The parameters of the porcine eyeball, Graefes Arch Clin Exp Ophthalmol, 249, pp. 475-482, 2011.

[11] C. Geuzaine and J. -F. Remacle, Gmsh: a three-dimensional finite element mesh generator with built-in pre- and post-processing facilities, International Journal for Numerical Methods in Engineering, 79(11), pp. 1309-1331, 2009.

[12] Z. Wang and S. Hirai, Finite element modeling and physical property estimation of rheological food objects, Journal of Food Research, Canadian Center of Science and Education, 1(1), pp. 48-67, Feb., 2012.